International Journal of Electrochemical Science 19 (2024) 100876

Contents lists available at ScienceDirect

International Journal of Electrochemical Science

journal homepage: www.editorialmanager.com/ijoes

Enhanced model for axisymmetric stability analysis of propagating circular defect-driven coating delamination under combined compressive and diffusion-induced stresses

M.H. Nazir [a,*], Z.A. Khan [b], Syed Zohaib Javaid Zaidi [c], Muhammad Majid Hussain [d], O.O. Taiwo [a]

[a] University of South Wales, Faculty of Computing, Engineering and Science, UK
[b] Bournemouth University, NCEM, Faculty of Science and Technology, UK
[c] Institute of Chemical Engineering and Technology, University of the Punjab, Lahore, Pakistan
[d] Herriot Watt University, UK

ARTICLE INFO

Keywords:
Delamination
Palladium coatings
Equi-biaxial compression
Circular delaminations
Diffusion-induced stress
Non-axisymmetric instabilities

ABSTRACT

This paper examines the delamination of palladium (Pd) coatings bonded to a steel substrate under equi-biaxial compression coupled with diffusion-induced stress. The study focuses on circular delaminations. Large delaminations cause the coating to debond, forming blisters, which generate a driving force on the edge crack tip. A two-part theoretical model is developed: axisymmetric blister propagation in a stable circular pattern and non-axisymmetric perturbation of the blister leading to branching. Detailed experimental studies validate the theoretical predictions. The experiments show that non-axisymmetric crack tip instabilities during propagation result in worm-like patterns.

1. Introduction

Protective coatings typically serve to mitigate the impact of physical and chemical attacks on the underlying substrate. However, under certain conditions, rather than impeding such attacks, these circumstances can actually encourage them, leading to the eventual separation of the coatings [1]. The occurrence of coating delamination can be attributed to various factors, with the primary problems being microscopic imperfections at the interface and the existence of pores within the coatings [2]. The issue of interfacial defects has long plagued coating systems, but it has recently gathered increased attention from the coatings industry. Numerous experts in the field have documented instances of premature failures and reduced coating lifespans attributable to these interfacial defects [3]. Therefore, it is vital to gain a comprehensive understanding of the delamination mechanism at the interface arising from defects, both in axisymmetric and non-axisymmetric propagation scenarios.

Compression-bonded coating on substrate delaminates due to residual stress coupled with diffusion induced stress is sufficiently high if an initial defect at interface exists. As the coating delaminates, the progression of interfacial debonding experiences mode-mix conditions. These conditions are contingent on five mode-mix parameters, governing both the rate of debonding propagation and its amplitude. The mode-mix parameters include the rate at which strain energy is release (G_o), debonding driving force (F), interface toughness function ($\sqrt{\mathbf{G_o/F}}$), detachment amplitude (w) and mode-mix function (j).

Both residual compressive stresses [4] and the diffusion induced stresses [5] effect the propagation and configurational stability of blisters. Various interfacial delamination morphologies evolve, including conventional-sided, circular, spiral (worm-like) and network-like blisters [6]. The most ubiquitous interfacial delamination is the spiral like, which typically occur at the coatings border [6,7] or blisters form due to delamination instability under critical coupling stress [8–11]. In addition, the telephone cord blisters have the tendency to bifurcate or merge and form a large variety of delamination patterns [12–16]. Up till now, the effect of bi-axial compression on the configurational strength at the inception of interfacial delamination has been theoretically addressed within the framework of von Karman nonlinear plate theory [17] for several limited cases with *no involvement* of diffusion induced stress [13, 18–21]. Improving comprehension of delamination morphologies can be achieved through an extension of analytical methods to encompass the impact of compressive residual stress in conjunction with stress

* Corresponding author.
E-mail address: hammad.nazir@southwales.ac.uk (M.H. Nazir).

https://doi.org/10.1016/j.ijoes.2024.100876
Received 28 May 2024; Received in revised form 11 November 2024; Accepted 11 November 2024
Available online 18 November 2024

Nomenclature

Notations	Description
$\vec{\nabla}\mu_k^Q$	gradient of chemical potential of specie k
$\vec{J}_k$	vector of diffusion flux of specie k
c_k	concentration of specie k
D_k	diffusion coefficient of specie k
R	molar gas constant
T	temperature
σ_m	stress tensor
σ_{di}	principle diffusion induced stresses
σ_{r_i}	principle residual stresses
$\overline{V_k}$	partial molar volumeof diffusing specie k
V_{m_k}	molar volume of solution
P	pressure
n_k	molar concentration of diffusing specie
h	coating thickness
l_c	coating length
b_c	coating width
s	substrate thickness
l_s	substrate length
b_s	substrate width
E_c, E_s	elastic moduli of coating and substrate respectively
α_c, α_s	coefficient of thermal expansion (CTE) of coating and substrate respectively
ΔT	change in temperature
t_b	location of bending axis corresponding to bending strain component being zero
ζ_r	radius of curvature of bilayer cantilever system due to residual stress
ζ_d	radius of curvature of bilayer cantilever system due to diffusion induced stress
$\boldsymbol{\sigma_d'/\sigma_{cr}}$	normalised stress
r	axisymmetric radius of a circular blister
σ_{cr}	critical stress
G′	elastic energy release rate
$f(\psi)$	dimensionless mode mix function
ψ	parameter defining mode II to mode I ratio of crack edge
λ	material parameter
M_c	bending moment of crack edge of coating
ΔN	resultant stress force acting on the coating
χ	dundur's elastic mismatch parameter
Γ_{IC}	mode I toughness
$\tilde{\mathbf{r}}$	perturbation radius
ε	perturbation parameter
F_1	fourier coefficient associated with ε

induced by diffusion.

When the coating expands more than the substrate due to heat, a positive temperature difference ($\Delta T > 0$) induces compression in the coating. This compression creates a residual compressive gradient that opposes the direction of diffusion [4,22–24]. The diffusion of specie is reduced due to the increasing residual compressive stress resulting in the delay in response to reach saturation point, according to the source [22]: 80 sec $< t <$ 2000 s. The maximum stress corresponding to saturation point is 130 MPa. The residual compressive stress remains within the substrate after external forces or loads have been applied and subsequently removed, then the effect diminishes once the diffusion reaches its saturation point according to [22–26]. This indicates that only at the start of exposure, before reaching the saturation state, the residual compressive stress affects the curvature of system. When the saturation of diffusion is reached, the resultant curvature becomes constant with no influence of residual stress. Therefore, for analysing the propagation and configurational stability of circular defects, our interest lies only before the saturation point considering the impact of the residual stress in conjunction with the dispersion induced stress [26]. Optical interferometry is employed to measure curvature, allowing for the deduction of feedback-diffusion induced stress in conjunction with the impact of residual compressive stress.

Therefore, our focus in analysing the propagation and configurational stability of blisters is specifically on the period before saturation, where the impact of residual compressive stress coupled with diffusion-induced stress is pronounced. During this pre-saturation phase, the initially circular defect spreads under increasing resultant curvature caused by coupled stresses. The blister expands while maintaining a relatively circular shape to a certain point at which a significant deviation from its circular symmetric pattern is observed. Also, further increase in resultant coupled stress makes the blister transforms into a worm-like configuration.

The paper clearly details the specific advancements made to the model by expanding the theoretical framework to incorporate the combined effects of residual compressive stress and diffusion-induced stress on the stability and propagation of circular delaminations in palladium-coated steel substrates. This enhancement addresses the complex interplay between these stresses, which was not previously considered, leading to a more accurate prediction of blister propagation and instability patterns. The improved model is validated against experimental data, demonstrating its ability to capture the transition from stable axisymmetric blister propagation to non-axisymmetric worm-like patterns, thereby offering a more comprehensive understanding of the delamination process under coupled stress conditions.

This research presents a continuation of the ongoing investigations within our research group, spanning from [27–48]. The current study is conducted within the context of thermodynamics combined with interfacial fracture mechanics. In the following section, an experimental analysis is carried out to examine the essential role played by crack front instabilities in the formation of telephone cord (worm-like) delamination under the influence of coupled stresses. The theoretical model predications which highlighted in the simulation aspect is being validated by the experiments. The subsequent section also presents the modelling of the destabilization of axisymmetric circular patterns in response to non-axisymmetric perturbations. The analysis of axisymmetric propagation yields a straightforward condition ensuring the prevention of interfacial delamination. This condition heavily depends on the mode-mix interfacial toughness. The predication for the loss of axisymmetric stable propagation shows an outstanding relationship between the quantitative and qualitative with experiments.

2. Experiment

2.1. Experimental setup

The experimental setup consists of a thin steel substrate coated with palladium Pd thin coating as shown in Fig. 1(a). Palladium (Pd) is chosen for the coating in this study due to its high coefficient of thermal expansion (CTE) and excellent thermal conductivity, essential for understanding stress mechanisms during delamination. Although not a common coating material, Pd is highly relevant in specific engineering applications where thermal management and expansion properties are critical. Its unique characteristics make it valuable for experimental studies on coating delamination, providing insights into the interactions between thermal and diffusion-induced stresses. This context emphasizes the study's significance in exploring failure mechanisms in

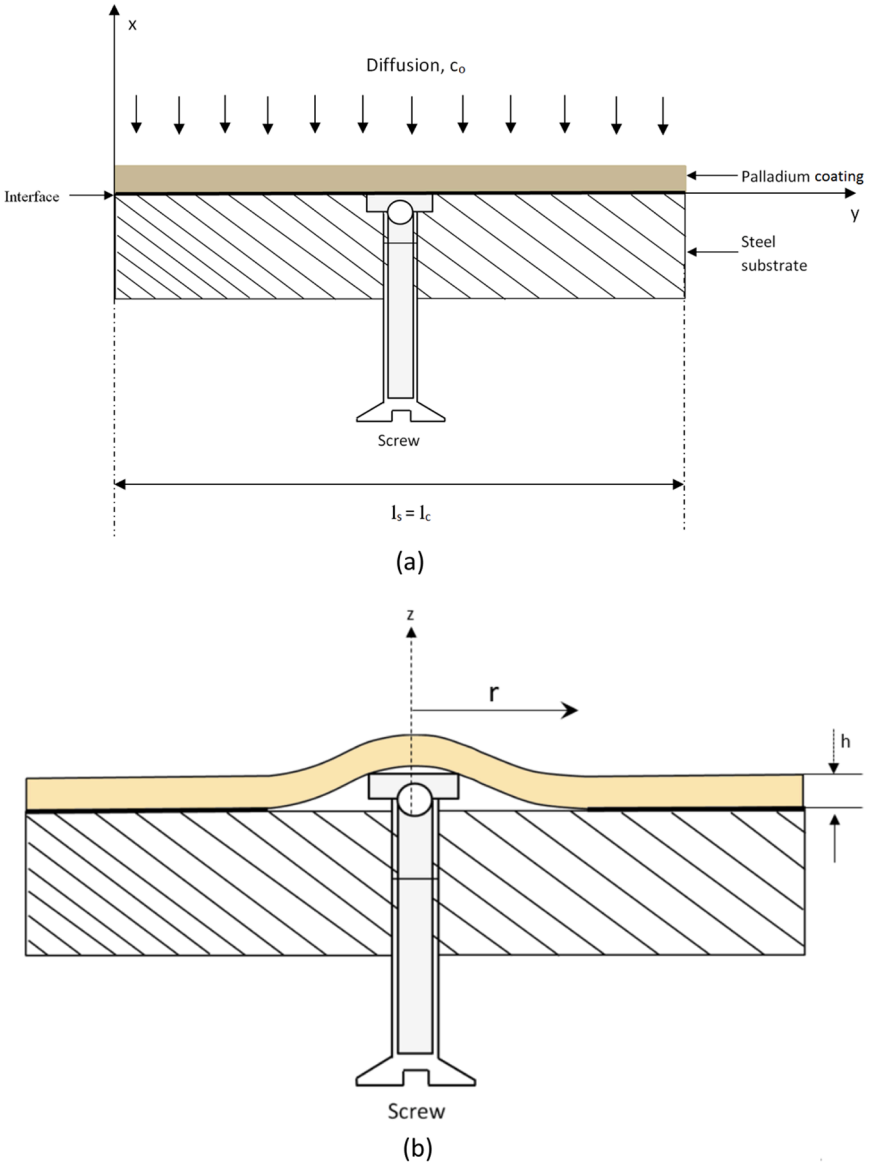

Fig. 1. (a) Schematic for the coating substrate system used in the experimental study. (b) A controlled circular defect (flaw) of radius r is introduced in to the interface between the Pd and steel by using a spherical ball tip screw through the backside of substrate.

advanced protective coatings, enhancing their reliability and performance in practical applications.

The Pd coating was applied by using a conventional spraying gun at temperature 318 K (45 °C). The thickness of the coating was h = 20 μm. The coefficients of thermal expansion (CTE) of palladium and steel are $\alpha_c = 12 \times 10^{-6}\,K^{-1}$ and $\alpha_s = 6.7 \times 10^{-6}\,K^{-1}$ respectively [49]. Young's moduli of palladium Pd and steel are 121 GPa [50] and 210 GPa [51] respectively. Poisson ratio for palladium Pd is 0.3 [50]. The coefficient of thermal expansion CTE and Young's modulus for the thin coating were measured by using thermomechanical analysis test according to the procedures of ASTM E831–14 and ASTM E2769 - 13 respectively. The coating was allowed to fully seal over a 24 hours period at 318 K before testing. The temperature 318 K is referred to as the fabrication temperature of coating-substrate system. Palladium Pd was chosen for the coating because of its high CTE and good thermal conductivity.

A controlled circular defect (flaw) is introduced into the interface between the Pd and steel (where the delamination event subsequently takes place) by using a spherical ball tip screw through the backside of substrate as shown in Fig. 1(b). Three defect sizes were created in three different coated samples and their delamination were observed. These three defect sizes were 5 μm, 25 μm and 45 μm respectively. This method has more merit, that any possible consequences of atmospheric pressure on the delamination of coating are decreased.

The experiment aimed to enhance the alignment with the assumptions of theoretical modelling by integrating stress caused by residual compressive and diffusion in Pd-coated steel samples featuring various defect radii (r). This systematic study investigated the sequence of events occurring when the residual compressive stress on the initial delamination region was elevated through heating the samples in the environmental chamber. Flaws with diverse initial radii were intentionally introduced at the border, and the models were subjected to chamber exposure to induce diffusion-induced stress concurrently with residual compressive stress. Video imaging recorded all events for subsequent analysis.

2.2. Experimental results

Three defect sizes 5 μm, 25 μm, and 45 μm, were created in three different Pd-steel coated samples. First, the smallest defects caused the catastrophic failure, resulting in the entire delamination of coating from

the substratum upon reaching the saturation condition of diffusion. This failure was recorded but is not shown here-in. A different (second type) behaviour, shown through a series of images, in Fig. 2(a) involves slightly larger defects, which ultimately results in the formation of "worm-like" pattern due to non-axisymmetric instabilities. The defect was initially created using spherical ball tip screw system with schematic shown in Fig. 2(b). The blisters propagated until saturation was reached and then arrested after saturation point due to constant curvature. The schematic of lobes (perturbations) of circular interface defect is shown in Fig. 2(c). As the blisters spread, the non-axisymmetric instabilities formed and gradually evolved into "worm-like" patterns which are commonly observed in the delamination of compressive coatings. Finally, a third type of behaviour with relatively large defects did not propagate at all. Again, this type of failure was recorded but is not shown here-in.

The results of blister propagation have been summarized in Fig. 3 highlighting Pd coating of varying thicknesses. Experimental results in Fig. 3 for the value of strain energy $G_0 = (1-\nu_c)h\sigma^2/E_c$ at which the point of delamination is graphed based on defects with different normalized blister radii r/h. Unfilled points show when blister expansion starts, while filled points indicate when "worm-like" behaviour emerges. Therefore, a separated open data point corresponds to an observation of catastrophic failure. The dashed line connecting an open point to a solid point illustrates the regions where the blisters were

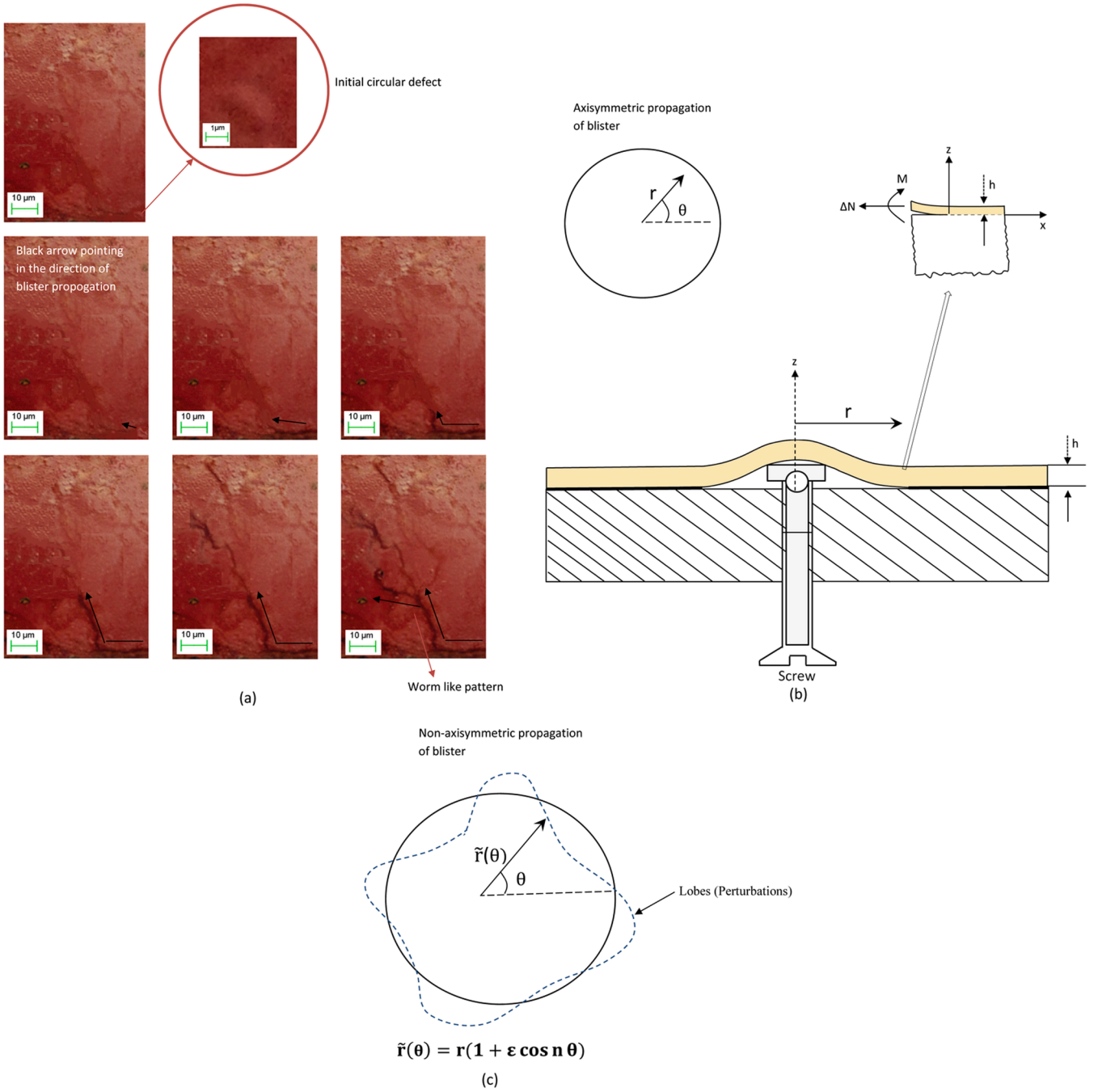

Fig. 2. (a) Sequence of images showing the propagation of an initially circular defect region under increasing resultant coupling stress (residual stress coupled with diffusion induced stress) (b) Conventions for axisymmetric circular blister and plain strain problem at edge of interfacial crack (c) Perturbations of circular interface defect.

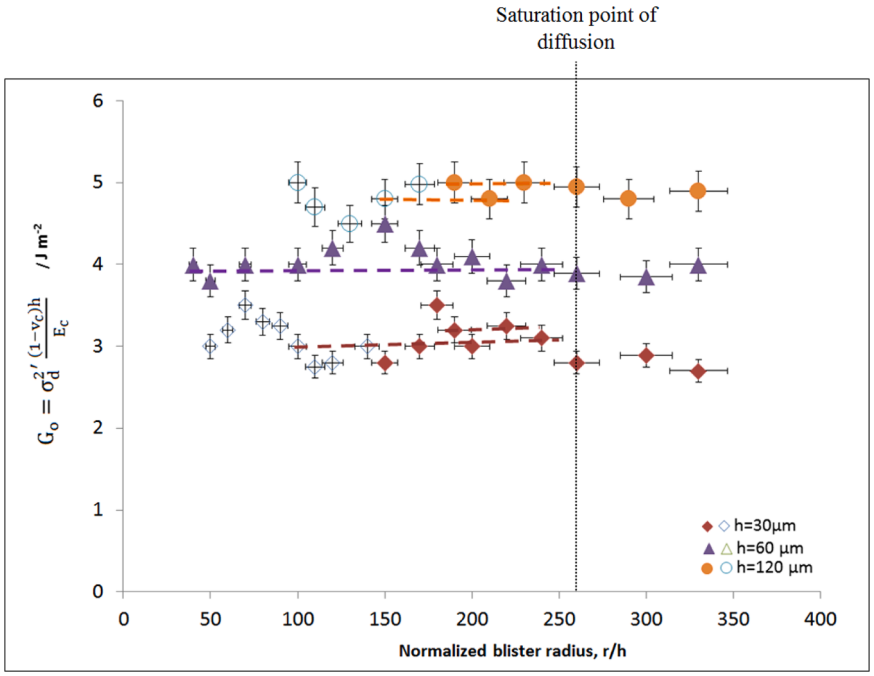

Fig. 3. Experimental results for the value $\mathbf{G_0 = (1-\nu_c)h\sigma^2/E_c}$ at which the delamination occurred is plotted as a function of the normalised radii of the defects.

observed to propagate. The propagation of blister was not observed after the saturation point of diffusion was achieved; therefore, the dashed line did not appear after the saturation point. The strain energy release rate G_0 seemed to rely on the thickness of the Pd coating therefore, $G_0 \approx$ 3 Jm-2 for h ≈ 60 μm, $G_0 \approx$ 4 Jm-2 for h ≈ 120 μm and $G_0 \approx$ 5 Jm-2 for h ≈ 30 μm.

The intention of this project was to establish a foundation for crafting a mathematical model (to be discussed in the following section), drawing insights exclusively from the recorded observations of the experiments. Therefore, making use of the data values in the above experiment from Fig. 3 and injecting them into the interface toughness function: $\sqrt{G_o/F} = \sigma_d\sqrt{[(1-\nu_c)h/(E_c \Gamma_{IC})]}$ [52] provides understanding into how mode mix conditions impact the behaviour of delamination. Here, σ_d depicts the diffusion induced stress that interacts with the residual compressive stress σ_r; F denotes the mode-adjusted crack driving force; mode I toughness Γ_{IC} appeared to vary with the thickness h of Pd coating, with Γ_{IC} ≈1.5 Jm^{-2} for h ≈ 120 μm, Γ_{IC} ≈0.6 Jm^{-2} for h ≈ 60 μm and $\Gamma_{IC} \approx$ 0.2 Jm^{-2} for h ≈ 30 μm [53]. The data

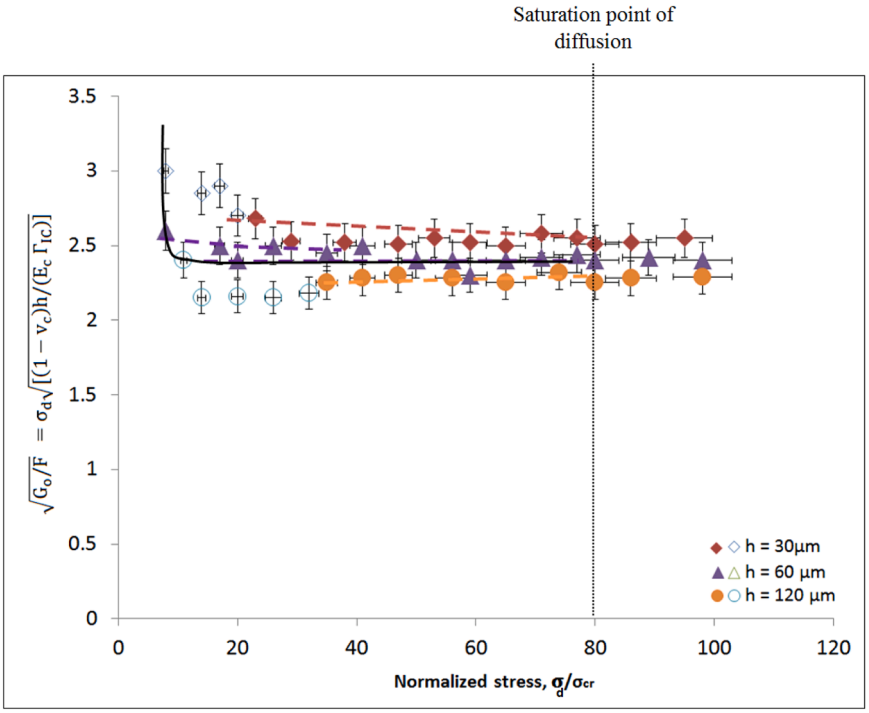

Fig. 4. The plot of the normalised interface toughness as a function of normalised stress. The data has been normalised by using equation: $\mathbf{\sqrt{G_o/F} = \sigma_d\sqrt{[(1-\nu_c)h/(E_c \Gamma_{IC})]}}$ and plotted as a function of normalised stress $\mathbf{\sigma_d/\sigma_{cr}}$.

has been normalised by using above equation of $\sqrt{G_o/F}$ and plotted as a function of normalised stress σ_d/σ_{cr}; where $\sigma_{cr} = 1.2 \quad E_c/(1-v_c^2)(h/r)^2$ [54] is the critical stress initiates at the start of coating delamination from the substratum. Utilizing the equation $\sqrt{G_o/F}$, the experimental data from Fig. 3 was employed to derive predictive data for the propagation conditions, illustrated in Fig. 4. Like Go, the interface toughness function $\sqrt{G_o/F}$ showed direct dependency on the coating thickness h $=120\ \mu$m showed the smallest toughness ($=\approx 2.2\ Jm^{-2}$) compared to the h $=30\ \mu$m with highest toughness ($=\approx 2.7\ Jm^{-2}$).

A further analysis was performed based on the number of lobes in non-axisymmetric blister propagation considering the impact of coupling stress while maintaining a constant defect radius, which has been plotted as a function of normalised stress σ_d/σ_{cr} in Fig. 5. It can be clearly seen that the number of lobes of blisters increased with increasing the normalised σ_d/σ_{cr}. However, contrary to the results in Figs. 3 and 4, there was no coating thickness effect observed in the results.

3. Mathematical model

The contribution in electrochemistry presented in this paper revolves around the study of delamination of coatings bonded to substrates, influenced by equi-biaxial compression coupled with diffusion-induced stress. The findings highlight how protective coatings, essential for shielding substrates from physical and chemical attacks, fail due to the diffusion of corrosive species towards the coating-substrate interface, resulting in electrochemical reactions. These reactions are aggravated by microscopic imperfections and pores at the interface.

The research develops a two-part theory: the axisymmetric propagation of blisters in a stable circular pattern and their transition into non-axisymmetric, worm-like patterns as delamination progresses. The study validates these theoretical predictions through detailed experimental analysis, demonstrating how residual compressive stress and diffusion-induced stress contribute to the configurational stability and propagation of blisters. This understanding is critical in addressing premature failures in protective coatings and enhancing their lifespan by mitigating interfacial defects.

The presented model is the continuation and advancements in our existing model [26]. Let us examine a scenario involving a non- uniform distribution of species within a sparse electrolyte solution. The force propelling the transport of the specie K is linked to the gradient of chemical potential $\vec{\nabla}\mu_k^Q$ [55]. The gradient of chemical potential $\vec{\nabla}\mu_k^Q$ exhibits direct proportion relationship with the vector of diffusion flux $\vec{J}_k$ of specie k as [56],

$$\vec{J}_k = -\frac{D_k c_k}{RT}\vec{\nabla}\mu_k^Q \tag{1}$$

Here, c_k denotes the intensity of specie k in a greatly diluted electrolyte solution; D_k stands for diffusion coefficient of specie k; R signifies the molar gas constant, while T represents temperature. Both sides of the equation are multiplied with $\vec{\nabla}$ while considering the law of conservation of mass ($\nabla.\vec{J_k} = -\frac{\partial c_k}{\partial t}$ [57]) yields the expression for Fick's second law as,

$$\frac{\partial c_k}{\partial t} = \vec{\nabla}.\left(\frac{D_k c_k}{RT}\vec{\nabla}\mu_k^Q\right) \tag{2}$$

Now consider the case of an elastic solid which is applied with an external mechanical force, the stress-supported diffusion may occur in the presence of stress fields. For an isotropic specie, the chemical potential μ_k^Q corresponding to stressed state of an elastic solid is given as [22],

$$\mu_k^Q = \mu_k - \int_0^{\sigma_m} \overline{V_k}\ d\sigma_m; \sigma_m = \frac{1}{3}\int_{i=1}^{i=3}\sigma_i \tag{3}$$

In this context, μ_k signifies, the chemical potential of specie k; σ_m signifies stress tensor which is same as the average of the summation of three principal stresses σ_i (i = 1, 2, 3). Each σ_i can be expressed as the sum of principal dispersion-induced stresses σ_{di} and principle residual stresses σ_{r_i} i.e. $\sigma_i = \sigma_{r_i} + \sigma_{d_i}$. $\overline{V_k}$ is a scaler term excluding the effect of the stress tensor, symbolising the partial molar volumeof diffusing specie k and obtained using Euler's first theorem for homogeneous functions [58].

$$\overline{V_k} = \left(\frac{\partial V_{m_k}}{\partial n_k}\right)_{T,P,n_k} = \left(\frac{V_{m_{k2}} - V_{m_{k1}}}{n_{k2} - n_{k1}}\right)_{T,P,n_{k\neq i}} \tag{4}$$

Here, $(\overline{V_k})$ relies on the alteration in molar volume of solution (V_{m_k}). This variation in molar volume V_{m_k} is contingent on temperature (T), pressure (P) and molar concentration of diffusing specie nk. In scenarios

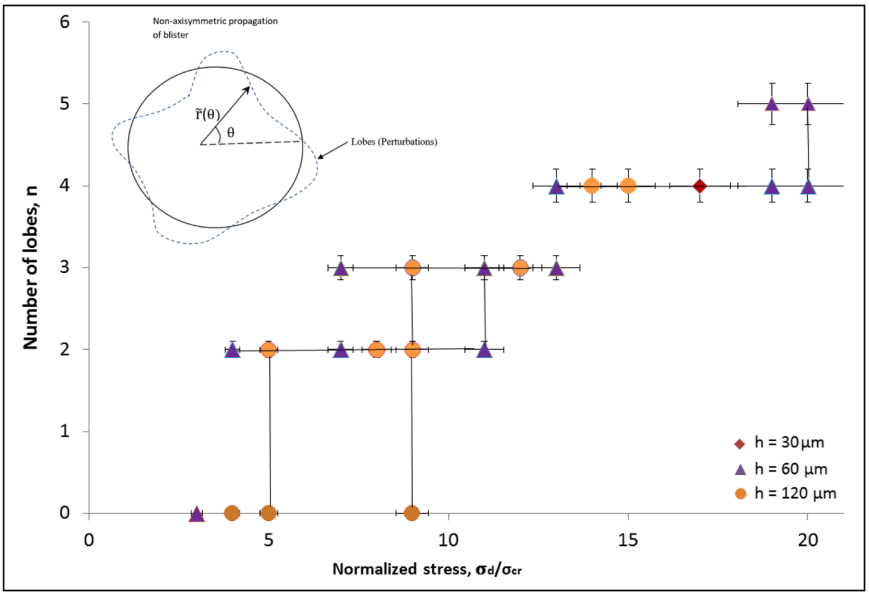

Fig. 5. The trends of the experimental results of the number of lobes of the blister propagating under the effects of coupled stress. The results are in agreements with the theoretical predications in Section 4.2.

of constant temperature (T) and pressure (P,) ($V_{m_{k_2}} - V_{m_{k_1}}$) represent the molar volume corresponding to the variation in molar concentration of diffusing specie k from n_{k1} to n_{k2} [59]. By solving Eq. 2 with the integration of Eq. 4 and eq. 3, the resulting diffusion equation of an elastic solid incorporates the collective impact of diffusion-induced stress and residual as,

$$\frac{\partial \mathbf{c_k}}{\partial \mathbf{t}} = \mathbf{D_k}\left\{\nabla^2 \mathbf{c_k} - \frac{\overline{\mathbf{V_k}}}{\mathbf{3RT}}\vec{\nabla}\mathbf{c_k}\vec{\nabla}\left[\int_{i=1}^{i=3}\left(\boldsymbol{\sigma}_{\mathbf{d}_i} + \boldsymbol{\sigma}_{\mathbf{r}_i}\right)\right] - \frac{\overline{\mathbf{V_k}}}{\mathbf{3RT}}\mathbf{c_k}\nabla^2\left[\int_{i=1}^{i=3}\left(\boldsymbol{\sigma}_{\mathbf{r}_i} + \boldsymbol{\sigma}_{\mathbf{d}_i}\right)\right]\right\} \tag{5}$$

With respect to the above elastic solid as a double layer's cantilever beam. Within this configuration, one coat is subjected to a dispersing species, maintaining a concentration denoted as c_o. In accordance with the current structural design configuration, the upper stratum of the bilayer cantilever beam acts as a coating, characterized by its dimensions—thickness (h), length l_c and width b_c .Simoultaneously, the lower stratum of the bilayer cantilever serves as a substrate, possessing dimensions in the form of thickness s, length l_s and width b_s as depicted. Establishing a reference point, our coordinate system defines the interface between the coating and substrate at x = 0. Additionally, it's imperative to note that the exposed plane of the coating and substratum are positioned at x = h and x = -s, correspondingly. Eq. 5 can be deployed to formulate the diffusion equations for coating considering the interplay of residual stress and diffusion induced stress as,

$$\frac{\partial \mathbf{c_{k_c}}}{\partial \mathbf{t}} = \mathbf{D_{kc}}\left\{\nabla^2 \mathbf{c_{k_c}} - \frac{\overline{\mathbf{V_{k_c}}}}{\mathbf{9RT}}\vec{\nabla}\mathbf{c_{kc}}\vec{\nabla}\left[\boldsymbol{\sigma}_{\mathbf{r_c}} + \boldsymbol{\sigma}_{\mathbf{d_c}}\right] - \frac{\overline{\mathbf{V_{k_c}}}}{\mathbf{9RT}}\mathbf{c_{k_c}}\nabla^2\left[\boldsymbol{\sigma}_{\mathbf{r_c}} + \boldsymbol{\sigma}_{\mathbf{d_c}}\right]\right\} \tag{6}$$

An established resolution for residual stress within a double layer beam as devised by Hseuh [60], is applicable for addressing the residual stress present in the coating. This residual stress in the coating arises from a disparity in the coefficient of thermal expansion (CTE) when the coating-substrate system undergoes temperature variations is outlined as,

$$\boldsymbol{\sigma}_{\mathbf{r_c}} = \mathbf{E_c}\left(\frac{(\mathbf{E_s}\boldsymbol{\alpha}_\mathbf{s}\mathbf{s} + \mathbf{E_c}\boldsymbol{\alpha}_\mathbf{c}\mathbf{h})\Delta\mathbf{T}}{(\mathbf{E_s s} + \mathbf{E_c h})} + \frac{\mathbf{x} - \mathbf{t_b}}{\boldsymbol{\zeta}_\mathbf{r}} - \boldsymbol{\alpha}_\mathbf{c}\Delta\mathbf{T}\right) \tag{7}$$

Here, E_c, E_s and α_c, and α_s represents the elastic moduli and coefficient of heat expansion (CTE) for the layer and substratum. ΔT denotes the temperature variation from the fabrication temperature or application temperature; $t_b = \frac{-E_s s^2 + E_c h^2}{2(E_s s + E_c h)}$ determines the position of bending axis where the bending strain component is zero; the variable x = t_b specifies the position of the neutral axis with zero strain; ζ_r represents the radius of curvature of bilayer cantilever system attributed to residual stress as [61],

$$\frac{1}{\zeta_r} = \frac{3\left[E_s s^2\left(\frac{(E_s\alpha_s s + E_c\alpha_c h)\Delta T}{(E_s s + E_c h)} - \alpha_s\Delta T\right) - E_c h^2\left(\frac{(E_s\alpha_s s + E_c\alpha_c h)\Delta T}{(E_s s + E_c h)} - \alpha_c\Delta T\right)\right]}{E_s s^2(2s + 3t_b) + E_c h^2(2h - 3t_b)} \tag{7(a)}$$

The equation for the normal stress induced by diffusion induced in a double layer beam, established by Zhang [62], provides a means to analyse the diffusion induced stress within the coating. As time progresses (t > 0), the diffusion of specie k initiates the accumulation of diffusion-induced stress within the coating, as expressed by the equation.

$$\boldsymbol{\sigma}_{\mathbf{d_c}} = \mathbf{E_c}\left(\frac{\mathbf{E_c h}\ \mathbf{V_{k_c}}\mathbf{c_{k_c}} + \mathbf{E_s s}\ \mathbf{V_{k_s}}\mathbf{c_{k_s}}}{\boldsymbol{3}(\mathbf{E_c h} + \mathbf{E_s s})} + \frac{\mathbf{x} - \mathbf{t_b}}{\boldsymbol{\zeta}_\mathbf{d}} - \frac{\mathbf{1}}{\mathbf{3}}\mathbf{c_{k_c}}\mathbf{V_{k_c}}\right) \tag{8}$$

In this context, c_{k_c}, c_{k_s} and V_{k_c}, and V_{k_s} denotes the concentration and partial molar volume of diffusing specie within coating and substrate respectively; ζ_d represent the radius of curvature of bilayer cantilever system due to diffusion induced stress as [22],

$$\frac{\mathbf{1}}{\boldsymbol{\zeta}_\mathbf{d}} = \frac{\mathbf{2}[\mathbf{E_c E_s hs}(\mathbf{h} + \mathbf{s})(\mathbf{V_{k_c}}\mathbf{c_{k_c}} - \mathbf{V_{k_s}}\mathbf{c_{k_s}})]}{\mathbf{E_c^2 h^4} + \mathbf{E_s^2 s^4} + \mathbf{2E_c E_s hs}(\mathbf{2h^2} + \mathbf{3hs} + \mathbf{2s^2})} \tag{8a}$$

Substituting the residual stress Eq. 7, eq. 7(a) and diffusion induced stress Eq. 8 and eq. 8(a) into Eq. 6 gives the relationship for the deformation of coating in consideration of the coupling effect of residual stress and diffusion induced stress as,

$$\frac{\partial \mathbf{c_{k_c}}}{\partial \mathbf{t}} = \left\{\left(\mathbf{D_{kc}} + \frac{\mathbf{D_{kc}E_c}\ \mathbf{V_{k_c}}^2}{\mathbf{9RT}}\ \mathbf{c_{k_c}}\right)\frac{\partial^2 \mathbf{c_{k_c}}}{\partial \mathbf{x^2}} + \frac{\mathbf{D_{kc}E_c}\ \mathbf{V_{k_c}}^2}{\mathbf{9RT}}\left(\frac{\partial \mathbf{c_{k_c}}}{\partial \mathbf{x}}\right)^2 - \frac{\mathbf{D_{kc}V_{k_c}}^2}{\mathbf{9RT}}\frac{\partial \mathbf{c_{k_c}}}{\partial \mathbf{x}}\left(\frac{\partial \boldsymbol{\sigma}_{\mathbf{r_c}}}{\partial \mathbf{x}} + \frac{\partial \boldsymbol{\sigma}_{\mathbf{d_c}}}{\partial \mathbf{t}}\right)\right\} \tag{9}$$

The influence of residual stress and the concentration of the diffusing species on stress generated by feedback diffusion can be determined by solving Eq. 9 as follows:

$$\boldsymbol{\sigma}_{\mathbf{d}}' = \frac{\partial \boldsymbol{\sigma}_{\mathbf{d_c}}}{\partial \mathbf{t}} = \frac{(\mathbf{9RT} + \mathbf{E_c}\mathbf{V_{k_c}}^2\mathbf{c_{k_c}})\ \frac{\partial^2 \mathbf{c_{k_c}}}{\partial \mathbf{x^2}} + \mathbf{E_c}\mathbf{V_{k_c}}^2\left(\frac{\partial \mathbf{c_{k_c}}}{\partial \mathbf{x}}\right)^2 - \frac{\partial \mathbf{c_{k_c}}}{\partial \mathbf{t}}\ \frac{\mathbf{9RT}}{\mathbf{D_{kc}}}}{\mathbf{V_{k_c}}^2\frac{\partial \mathbf{c_{k_c}}}{\partial \mathbf{x}}} - \frac{\partial \boldsymbol{\sigma}_{\mathbf{r_c}}}{\partial \mathbf{x}} \tag{10}$$

3.1. Axisymmetric propagation of blister – stable growth in a "circular" pattern

The condition for axisymmetric propagation of a circular blister is derived in this sub section. This section considers the possibility for the circular blister to propagate in a uniform circular shape. Eq. 10 **can be employed to calculate the effect of residual stress and feedback-diffusion induced stress near crack tips. These crack tips can reside near the regions of defects in the coating which can incubate the delamination of coating. The conventional form of normalised stress (**$\frac{\sigma_d'}{\sigma_{cr}} = \frac{(1-v_c^2)}{E_c}\ \sigma_d'\left(\frac{r}{h}\right)^2$ [63]**), can now be modified as,**

$$\frac{\sigma_d'}{\sigma_{cr}} = \frac{(1-v_c^2)}{E_c}\left(\frac{(9RT + E_c {V_{k_c}}^2 c_{k_c})\ \frac{\partial^2 c_{k_c}}{\partial x^2} + E_c {V_{k_c}}^2 \left(\frac{\partial c_{k_c}}{\partial x}\right)^2 - \frac{\partial c_{k_c}}{\partial t}\ \frac{9RT}{D_{k_c}}}{{V_{k_c}}^2 \frac{\partial c_{k_c}}{\partial x}} - \frac{\partial \sigma_{r_c}}{\partial x}\right)\left(\frac{r}{h}\right)^2 \tag{11}$$

Where r denotes the axisymmetric radius of a circular blister, as illustrated in Fig. 2(b). This study is centred around the circular interface crack that emerges at the meeting point of the coating and substrate. It is important to highlight that σ_{cr} denotes the critical stress, indicating the stress threshold at which the delamination of the coating from the substrate initiates, in both plane strain and axisymmetric modes. This has been detailed in the provided reference [64]. It is essential to recognize that σ_{cr} is affected by the radius of the circular interface crack that develops between the coating and the substrate. Notably, a larger crack radius 'r' at this interface leads to a reduced value of σ_{cr}, whereas, a smaller crack radius r corresponds to an increased σ_{cr}. Consequently, it is imperative to highlight that the ratio σ_d'/σ_{cr} can escalate either due to increase in σ_d' or due to an enlargement in blister radius 'r'.

The crack propagation's driving force adaptation hinges on the elastic energy release rate G′ and a dimensionless mode mix function f(ψ), [63,65]

$$F = \frac{G}{f(\psi)} \tag{12}$$

Where,

$$G = \frac{6(1-v_c^2)}{E_c h^3}\left[M_c^2 + \frac{1}{12}h^2 \Delta N^2\right] \tag{12a}$$

$$f(\psi) = \sec^2[(1-\lambda)\psi] \tag{12b}$$

$$\psi = \frac{K_2}{K_1} = \cot\frac{\cos\omega + \left[\frac{h\Delta N}{\sqrt{12}M_c}\right]\sin\omega}{\left[\frac{h\Delta N}{\sqrt{12}Mc}\right]\cos\omega - \sin\omega} \tag{12c}$$

$$h\Delta N \Big/ \sqrt{12}M_c = 0.2(1+v_c)\sqrt{\left(\frac{1}{0.2(1+v_c)+0.2(1-v_c^2)}\left(\frac{\sigma_d'}{\sigma_{cr}} - 1\right)\right)} \tag{12d}$$

In this context, ψ represents a factor that characterizes the ratio of mode II to mode I at the crack edge; λ depicts the material parameter and best fit λ occurs within around 0.3 for Pd coated steel sample [66]; M_c is the bending moment of crack edge of coating; ΔN is the resultant stress force acting on the coating; Parameter ω in Eq. 12(c) is dependent upon Dundur's elastic mismatch parameter χ [67]. Where $\chi = (\overline{E_c} - \overline{E_s})/(\overline{E_c} + \overline{E_s})$ [68].

From Eq. 12(a), eq. 12(b) and Eq. 12(c), it is evident that G, f(ψ) and ψ at the boundary of crack rely on the combination of relationship $h\Delta N/\sqrt{12}M_c$ in Eq. 12(d), the term being the function of normalised feedback-diffusion induced stress σ_d'/σ_{cr}. After changes, Hutchinson's equations for G, f(ψ) and ψ may undergo adjustment to redefine the problem of delamination propagation by considering stress induced through feedback diffusion.

The condition for the incipient fracture to propagate is $F = \Gamma_{IC}$ [52], where Γ_{IC} is mode I toughness as discussed in Section 2. By incorporating feed-back diffusion induced stress and incipient condition $F = \Gamma_{IC}$, it is possible to find the incipient spread of circular blister for the family of interface toughness function as, [52]

$$\sqrt{\frac{G_o}{F}} = (1-v_c)h = \sigma_d'\sqrt{\left[\frac{(1-v_c)h}{E_c\ \Gamma_{IC}}\right]};\ G_o = \sigma_d^{2'}\frac{(1-v_c)h}{E_c} \tag{13}$$

The expression's left side is contingent on σ_d'/σ_{cr}; this resultant equation adopts a structure akin to that employed in experimental Section 2, facilitating the fitting of experimental data values from Fig. 2 and the generation of curves in Fig. 3 depicting the initial expansion of a circular blister. Additionally, Eq. 13 proves valuable in enabling a quantitative comparison between experimental observations and theoretical predictions.

3.2. Non- axisymmetric propagation of blister – unstable growth in "worm-like" pattern

In this sub-section, condition for the non-axisymmetric propagation of the circular blister is derived. This section considers two major possibilities for the circular blister to propagate in a non-circular shape.

First possibility analysed is *the non-axisymmetric propagation from the nonlinear axisymmetric state, while the interface crack remains circular* in shape. It has been reported [66] that the branching in to a non-axisymmetric mode do not occur until $\sigma_d'/\sigma_{cr} = 55.6$ for the condition when poisons ratio of coating, $v_c = 0.3$.

The other possibility for the non-axisymmetric propagation is *the instability to the perturbation of the circular crack front* as shown in Fig. 2 (c). According to the Fig. 2(c), the perturbation in crack front can be

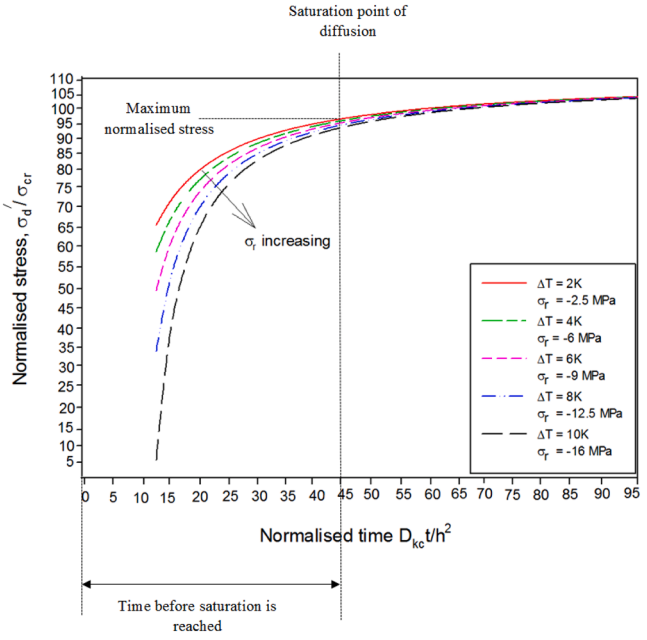

Fig. 6. Figure showing that resulting response to reach the saturation point is delayed with increasing the residual compressive stress. The effect of residual compressive stress fades away after saturation and the resultant stress affecting the curvature becomes constant.

considered in the form as, [69]

$$\tilde{\mathbf{r}}(\boldsymbol{\theta}) = \quad \mathbf{r} \quad (\mathbf{1} + \boldsymbol{\varepsilon}\mathbf{cosn}\boldsymbol{\theta}) \tag{14}$$

In this context, ε signifies the perturbation parameter; and n denotes the number of modes ranging from n=1 to n=8; the variation of θ corresponding to lowest mode follows the pattern cosnθ

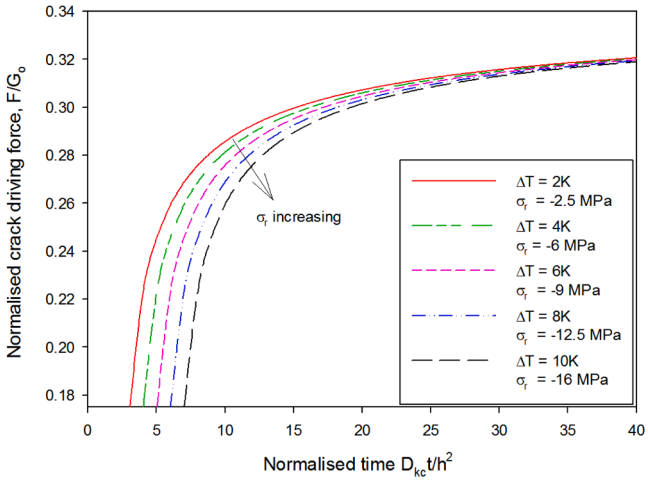

Fig. 7. Mode adjusted crack driving force F at the edge of circular blister as a function of normalised time. The plot shows that, above a certain value of time, the crack driving force **F** diminishes with increasing time. The trends in plot also show that the response of crack driving force F is delayed with increasing the residual compressive stress.

Where,

$$G_1 = \frac{6(1-v_c^2)}{E_c h^3}\left[MM_1 + \left(\frac{h^2}{12}\right)\Delta N \Delta N_1\right] \tag{16a}$$

$$\Psi_1 = -\left(\frac{h}{\sqrt{12}}\right)\left\{1 + \left[\frac{h\Delta N}{\sqrt{12}M}\right]^2\right\}^{-1}[M\Delta N_1 - \Delta N M_1]M^{-2} \tag{16b}$$

$$M_1 = \frac{6(1-v_c^2)}{E_c h^3}\left(\frac{h}{r^2}\right)\left\{\left[-\left[6(1-v_c^2)\right]^{-\frac{1}{2}} \quad \left[6(1-v_c^2)\right]^{\frac{1}{2}} r^{-1} w'\right]' - \left[\left[6(1-v_c^2)\right]^{-\frac{1}{2}} \quad \left[6(1-v_c^2)\right]^{\frac{1}{2}} r^{-1} w'\right]''\right\} \tag{16c}$$

with n=8. This type of configurational instability in delamination has been previously addressed in experimental Section 2 . The emergency of "worm like" blisters as observed in experimental Section 2 is believed to be explained by the tendency of the perturbation crack front to exhibit instability along its length. In contrast, the stable crack front of the circular blister provides with the lower level of perturbation in the crack driving force compared to an unstable crack front. This can be equated by using the concept of first-order perturbation theory as, [70,71]

$$\mathbf{F} = \quad \mathbf{F_o}\left(\frac{\boldsymbol{\sigma_d}'}{\boldsymbol{\sigma_{cr}}}\right) + \boldsymbol{\varepsilon}\mathbf{F_1}\left(\frac{\boldsymbol{\sigma_d}'}{\boldsymbol{\sigma_{cr}}}, \mathbf{n}\right)\mathbf{cosn}\ \boldsymbol{\theta} \tag{15}$$

Here, F_o stands for the established solution of F in an axisymmetric state; F_1 denotes the Fourier coefficient linked to ε. By selecting suitable value for f(ψ), elastic mismatch parameters, and other dependencies, both F_o and F_1 can be tailored accordingly. The stability of the circular crack front determined by a given n, hinges on the sign of F_1.The derivation of F_1 in $\varepsilon F_1 \cos n\theta$, presented as a perturbation solution, is achieved by applying Eigen-value solution to Eq. 12 as,

$$\mathbf{F_1} = \mathbf{f^{-1}G_1} - \mathbf{f^{-2}G}\left(\frac{\mathbf{df}}{\mathbf{d\psi}}\right)\boldsymbol{\psi_1} \tag{16}$$

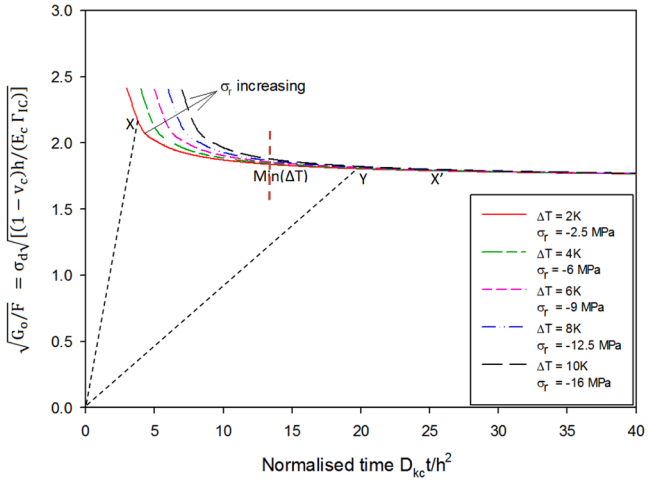

Fig. 8. Normalised time associated with initial propagation of circular blister for the family of residual compressive stress values.

$$w = w^{(0)}(r) + \varepsilon w^{(1)}(r)\cos n\theta \tag{16d}$$

$$\Delta N_1 = 12\left(\frac{6(1-v_c^2)}{E_c h^3}\left(\frac{1}{r^2}\right)\right)\left[-\frac{N}{12} + \left(-\frac{N}{12}\right)'\right] \tag{16e}$$

The quantities other than M_1, w and ΔN_1 in the expressions for F_1, G_1 and ψ_1 are calculated in the axisymmetric state; w in Eq. 16(c) denotes the normal component of displacement of coating and is sought in the form of non-axisymmetric perturbation in Eq. 16(d).

The incipient condition for the crack front to propagate is maintaining a constant value of F according to $F = \Gamma_{IC}$. Therefore, if F_1 returns a *negative* value for a given n, the perturbation is *stable*, in a manner that the outward boundary of crack front has lower value of F compared to the innermost data points along the front. This behaviour will account for the stable growth of blister in a circular pattern. Contrary to this, if F_1 returns a *positive* value, the outward boundary of crack front has higher value of F, and the perturbation is *unstable*. This behaviour will account for the blister to be driven further away from the circular shape resulting in non-axisymmetric propagation.

4. Simulation results and discussion

This section investigates the numerical simulation, utilizing the finite variation method, to explore the impact of residual compressive stress and diffusion-induced stress on blister propagation. Recent published papers investigating the combined effect of compressive and diffusion induced stresses on axis-symmetric stability of propagating blisters are [72,73].

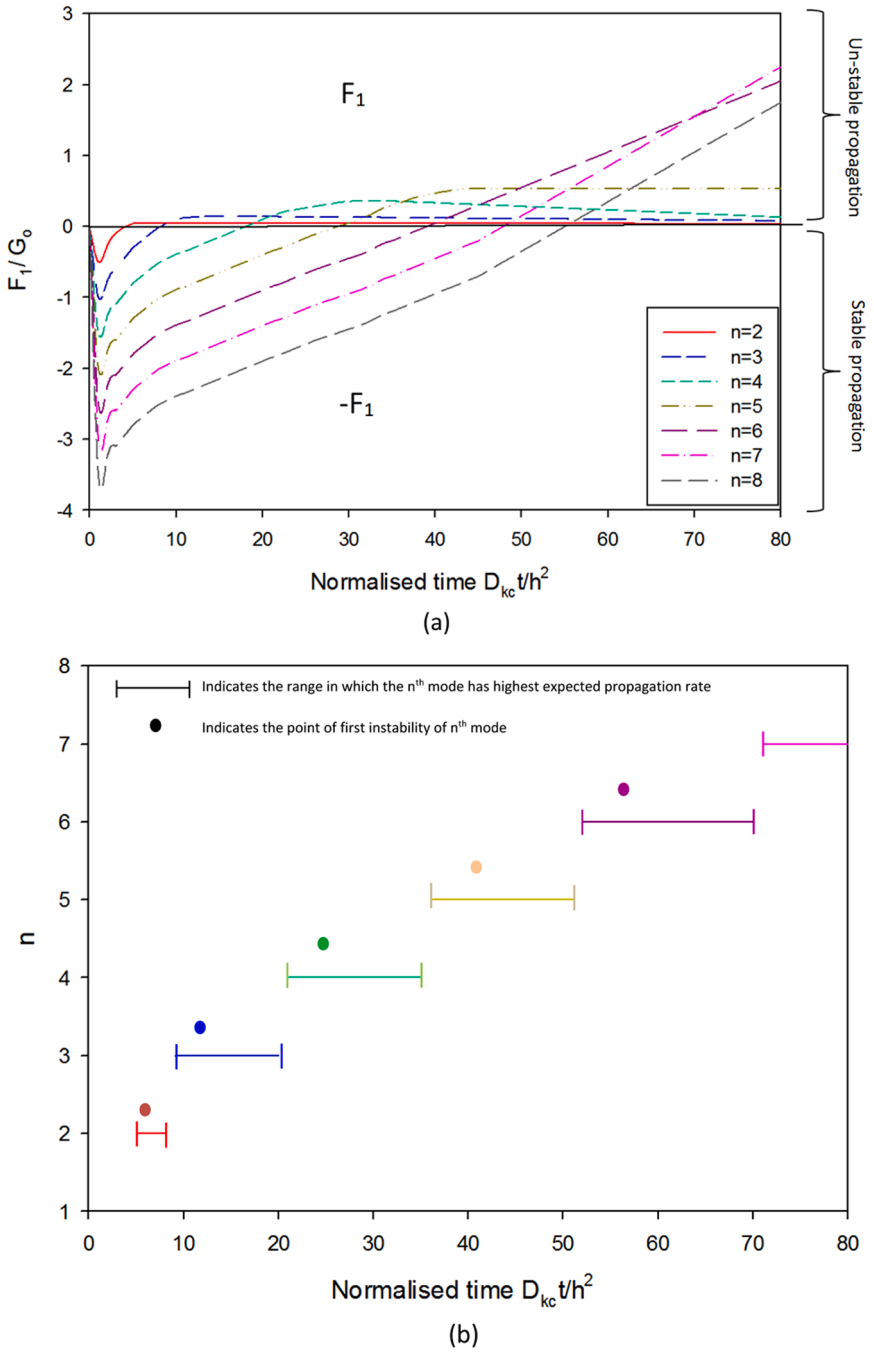

Fig. 9. (a) F_1/G_o as a function of σ'_d/σ_{cr} for various modes from n= 2 to n= 8 (b) Instability of modes derived from data in Fig. 9(a).

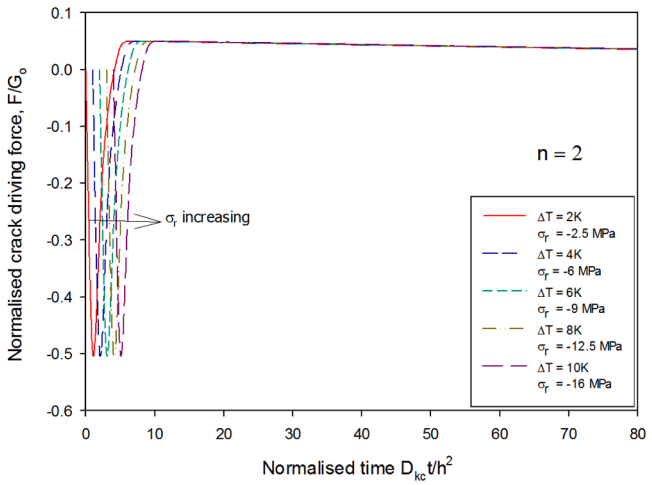

Fig. 10. The trends in plot show that the response of F_1 is delayed with increasing the residual compressive stress, consider n = 2.

Based on numerical simulations using the finite difference method, this section discusses the impact of compressive residual stress coupled with diffusion-induced stress on the nucleation and propagation of blisters in coatings with defects. In the numerical analysis, all dimensional parameters in the equations were normalized, including the normalised stress, normalised time, and normalised crack driving force.

The simulation predictions have been validated through comparison with experimental results. These validations are discussed in the next two sections, along with the results discussion.

4.1. Axisymmetric propagation of blister

To illustrate the axisymmetric propagation of blister, comparison of the predicted normalised stress σ_d'/σ_{cr} from various values of residual stress σ_r are first carried out as a function of normalised time $Dk_c\ t/h^2$ and shown in Fig. 6. As assumed, the residual compressive stress σ_r has a significant impact on normalised stress when the normalised time $D_{kc}t/h^2$ is less than 45. However, once the diffusion reaches its saturation point, the influence of the residual compressive stress on the normalized stress will diminish, meaning, $D_{kc}t/h^2 > 45$. The maximum normalised stress corresponding to the point of saturation is ~ 100. As the effect of residual compressive stress is dominant in period: $5 < D_{kc}t/h^2 < 45$ therefore, this period, along with the corresponding normalised stress values is critical for blister propagation and will be utilised in simulation. From Fig. 6, the resulting response to reach the saturation point is delayed with increasing the residual compressive stress.

In Fig. 7, the impact of residual compressive stress on normalised mode adjusted crack driving force F/Go is depicted for an unsaturated time range $D_{kc}t/h^2 < 45$ in Fig. 7. The plot illustrates that beyond a specific time threshold, the crack driving force F diminishes with time progression. Consequently, a propagating circular blister to the right of a maximum point is stable and axisymmetric. However, the potential for non-axisymmetric instability, discussed in the following section remains. The plot trends also indicate a delayed response in the crack driving force F with increasing the residual compressive stress.

An enhanced graph displays factors governing blister propagation, described in terms of interface toughness function $\sqrt{G_o/F} = \sigma_d' \sqrt{[(1-\nu_c)h/(E_c\ \ \Gamma_{IC})]}$ as shown in Fig. 8. For this discussion, consider the plot for $\Delta T = 2K$ in Fig. 8. Assume an initial circular flaw, with fixed coating thickness h, loaded by increasing σ_d' over time until saturation. This loading is represented by a straight trajectory in Fig. 8. If the parameters are such that, the trajectory is one-like OX, which intersects the curve for circular crack propagation to the left of minima, then the blister will undergo an unstable advance until it arrests at X'. With further increasing σ_d', the crack propagates in a stable manner with σ_d'/σ_{cr} increasing. However, if the trajectory is one-like OY, which intersects the curve for circular crack propagation to the right of minima, then the blister will undergo a stable advance right from the start. Note that the minima in Fig. 8 is obtained at $\sigma_d'/\sigma_{cr} \approx 2$. Let Min (ΔT) denote the minima on the propagation curve for a given ΔT, then there will be no blister propagation irrespective of the initial size of defect if, $\sigma_d'\sqrt{[(1-\nu_c)h/(E_c\ \ \Gamma_{IC})]} < \text{Min}(\Delta T)$ as shown in Fig. 8. This limit provides with the guideline in terms of deposition of thin coatings, as it guarantees that the delamination will not occur, even as circular blisters. It is possible to find the radius of circular defect $r^* \approx 1.1h[(1-\nu_c)E_c h/\text{Min}^2(1-\nu_c^2)^2\Gamma_{IC}]$ against this minima, such that if, $r << r^*$, the defect will be categorised as very small with no hazard of propagating.

The theoretical prediction for propagation conditions in Fig. 8 on comparison with the experimental curves in Fig. 4 showed an excellent agreement.

4.2. Non- axisymmetric propagation of blister

For the stability analysis of perturbations using perturbation theory, the curves for F_1/G_o as a function of normalised time are plotted in Fig. 9 (a) for modes: n = 2 up to n = 8, for the case when ΔT = 2 K. For the lowest order in perturbation parameter ε, the solution for n = 1 returned $F_1 = 0$, meaning that the initial defect will not propagate at all, which is of no particular interest according to the theme of paper. The propagation curves show that, if F_1 returns a negative value for a given n, the perturbation is stable, and accounts for the stable growth of blister in a circular pattern. However, if F_1 returns a positive value, the perturbation is unstable, and account for the blister to be driven further away from the circular shape resulting in non-axisymmetric propagation. The normalised time at which each mode becomes unstable is indicated by a solid dot in Fig. 9(b). In the same figure, the range indicates the region where the nth mode has highest F_1 among all the other modes. For the purpose of illustration, consider the plot for n = 2 in Fig. 10. The trends in plot show that the response of F_1 is delayed with increasing the residual compressive stress. Similar delay in response can also be seen for the plots with n= 3 to n=8, not shown herein.

This paper focuses on the delamination of palladium (Pd) coatings on steel substrates under equi-biaxial compression and diffusion-induced stress, highlighting its strengths and limitations compared to existing methods. It is ideal for analyzing systems with significant compressive residual and diffusion-induced stress, leading to blister formation and propagation. The theoretical model developed provides a detailed understanding of blister propagation, validated by comprehensive experimental data, offering a robust framework for predicting and mitigating failure mechanisms in Pd-coated steel. However, its application is limited, as different coating-substrate systems may exhibit distinct failure mechanisms not fully addressed by this model. While it offers significant insights into Pd-steel systems, further refinement is needed for other combinations. The main strength is its detailed coupling of mechanical and diffusion-induced stresses, but the weakness is its limited generalizability to other material systems without further adaptation.

5. Conclusions

This paper introduces two primary forms of defect-driven delamination influenced by compressive residual and diffusion-induced stresses. Initial investigations establish a theory for the expansion of an axisymmetric blister, considering equi-biaxial compressive stress along with feedback diffusion-induced stress. Then the second calculations generated the results that the blister can propagate, such that it can become unstable with the lower level of perturbation in the crack driving force. When applied with appropriate conditions, the blister

loses its axisymmetric nature and propagates in a manner that it develops lobes around its boundaries; the intensity of which depends on the magnitude of time dependent normalised stress σ_d'/σ_{cr} . This unstable propagation of blister may result in the development of "worm-like" patterns which are often observed in the delamination of thin coatings. The theoretical model is based on the observations recorded from the experimentation. The experiments conducted in this study have provided substantial support for the theoretical predictions outlined in the simulation section of the paper.

CRediT authorship contribution statement

Muhammad Majid Hussain: Resources. **O O Taiwo:** Writing – review & editing, Writing – original draft, Visualization. **Syed Zohaib zaidi:** Methodology, Conceptualization. **Mian Hammad Nazir:** Validation, Resources, Methodology, Investigation. **Zulfiqar Khan:** Methodology.

Declaration of Competing Interest

The authors declare that they have no known competing financial interests or personal relationships that could have appeared to influence the work reported in this paper.

References

[1] J.M. Pommersheim, T. Nguyen, K. Hartzfeld, Prediction of blistering in coating systems, ACS Symp. . Ser. 689 (1998) 137–150, https://doi.org/10.1021/bk-1998-0689.ch010.

[2] T. Nguyen, J. Hubbard, J. Pommersheim, Unified model for the degradation of organic coatings on steel in a neutral electrolyte, J. Coat. Technol. 68 (1996) 45–56, https://doi.org/10.1007/BF02698267.

[3] M. Morcillo, Soluble salts: their effect on premature degradation of anticorrosive paints, Prog. Org. Coat. 36 (1999) 137–147, https://doi.org/10.1016/S0300-9440(99)00030-7.

[4] S. Ho, C. Hillman, F. Lange, Z. Suo, Surface cracking in layers under biaxial, residual compressive stress, J. Am. Ceram. Soc. 78 (1995) 2353–2359, https://doi.org/10.1111/j.1151-2916.1995.tb08604.x.

[5] Y.-T. Cheng, M.W. Verbrugge, The influence of surface mechanics on diffusion-induced stresses within spherical nanoparticles, J. Appl. Phys. 104 (2008) 083521, https://doi.org/10.1063/1.2990039.

[6] Y. Ni, A.K. Soh, On the growth of buckle-delamination pattern in compressed anisotropic thin films, Acta Mater. 69 (2014) 37–46, https://doi.org/10.1016/j.actamat.2014.01.047.

[7] K. Pan, Y. Ni, L. He, Effects of interface sliding on the formation of telephone cord buckles, Phys. Rev. E 88 (2013) 062405, https://doi.org/10.1103/PhysRevE.88.062405.

[8] J. Bedrossian, R.V. Kohn, Blister patterns and energy minimization in compressed thin films on compliant substrates, Commun. Pure Appl. Math. 68 (2015) 472–510, https://doi.org/10.1002/cpa.21522.

[9] B. Audoly, B. Roman, A. Pocheau, Secondary buckling patterns of a thin plate under in-plane compression, Eur. Phys. J. B-Condens. Matter Complex Syst. 27 (2002) 7–10, https://doi.org/10.1140/epjb/e20020123.

[10] H. Chai, C.D. Babcock, W.G. Knauss, One-dimensional modelling of failure in laminated plates by delamination buckling, Int. J. Solids Struct. 17 (1981) 1069–1083, https://doi.org/10.1016/0020-7683(81)90082-4.

[11] G. Parry, J. Colin, C. Coupeau, F. Foucher, A. Cimetière, J. Grilhé, Effect of substrate compliance on the global unilateral post-buckling of coatings: AFM observations and finite element calculations, Acta Mater. 53 (2005) 441–447, https://doi.org/10.1016/j.actamat.2004.10.026.

[12] M. Moon, H.M. Jensen, J.W. Hutchinson, K. Oh, A. Evans, The characterization of telephone cord buckling of compressed thin films on substrates, J. Mech. Phys. Solids 50 (2002) 2355–2377, https://doi.org/10.1016/S0022-5096(02)00007-5.

[13] M.-W. Moon, K.-R. Lee, K.-H. Oh, J.W. Hutchinson, Buckle delamination on patterned substrates, Acta Mater. 52 (2004) 3151–3159, https://doi.org/10.1016/j.actamat.2004.03.029.

[14] Abdallah, P. Bouten, J. Den Toonder, G. de With, The effect of moisture on buckle delamination of thin inorganic layers on a polymer substrate, Thin Solid Films 516 (2008) 1063–1073, https://doi.org/10.1016/j.tsf.2007.06.119.

[15] M. Cordill, D. Bahr, N. Moody, W. Gerberich, Adhesion measurements using telephone cord buckles, Mater. Sci. Eng.: A 443 (2007) 150–155, https://doi.org/10.1016/j.msea.2006.08.059.

[16] S.-J. Yu, L. Zhang, Y. Zhao, Z. Du, Transitions from straight-sided to telephone cord buckles in SiAlNx films, Thin Solid Films 550 (2014) 480–485, https://doi.org/10.1016/j.tsf.2013.11.080.

[17] J. Reddy, A refined nonlinear theory of plates with transverse shear deformation, Int. J. Solids Struct. 20 (1984) 881–896, https://doi.org/10.1016/0020-7683(84)90060-7.

[18] L.B. Freund, S. Suresh, Thin film materials: stress, defect formation and surface evolution, Cambridge University Press, 2004, https://doi.org/10.1017/CBO9780511754715.

[19] B. Audoly, Stability of straight delamination blisters, Phys. Rev. Lett. 83 (1999) 4124, https://doi.org/10.1103/PhysRevLett.83.4124.

[20] Z. Chen, B. Cotterell, W. Wang, E. Guenther, S.-J. Chua, A mechanical assessment of flexible optoelectronic devices, Thin Solid Films 394 (2001) 201–205, https://doi.org/10.1016/S0040-6090(01)01185-7.

[21] M. Zhao, J. Zhou, F. Yang, T. Liu, T.-Y. Zhang, Effects of substrate compliance on circular buckle delamination of thin films, Eng. Fract. Mech. 74 (2007) 2334–2351, https://doi.org/10.1016/j.engfracmech.2007.01.016.

[22] F.-Z. Xuan, S.-S. Shao, Z. Wang, S.-T. Tu, Influence of residual stress on diffusion-induced bending in bilayered microcantilever sensors, Thin Solid Films 518 (2010) 4345–4350, https://doi.org/10.1016/j.tsf.2009.12.002.

[23] X. Liu, G. Frankel, Effects of compressive stress on localized corrosion in AA2024-T3, Corros. Sci. 48 (2006) 3309–3329, https://doi.org/10.1016/j.corsci.2006.01.010.

[24] X. Zhao, P. Munroe, D. Habibi, Z. Xie, Roles of compressive residual stress in enhancing the corrosion resistance of nano nitride composite coatings on steel, J. Asian Ceram. Soc. 1 (2013) 86–94, https://doi.org/10.1016/j.jascer.2013.09.005.

[25] W.-Y. Chu, J. Yao, C.-M. Hsiao, Stress corrosion cracking of austenitic stainless steel under compressive stress, Corrosion 40 (1984) 302–306, https://doi.org/10.5006/1.3579747.

[26] M. Nazir, Z.A. Khan, A. Saeed, K. Stokes, Modeling the effect of residual and diffusion-induced stresses on corrosion at the interface of coating and substrate, Corrosion 72 (2016) 500–517, https://doi.org/10.5006/1970.

[27] M.H. Nazir, Z.A. Khan, A. Saeed, K. Stokes, A predictive model for life assessment of automotive exhaust mufflers subject to internal corrosion failure due to exhaust gas condensation, Eng. Fail. Anal. 63 (2016) 43–60, https://doi.org/10.1016/j.engfailanal.2016.02.008.

[28] M.H. Nazir, Z.A. Khan, K. Stokes, A holistic mathematical modelling and simulation for cathodic delamination mechanism – A novel and efficient approach, J. Adhes. Sci. Technol. 1 (2015) 39, https://doi.org/10.1080/01694243.2014.999184.

[29] M.H. Nazir, Z. Khan, K. Stokes, Modelling of metal-coating delamination incorporating variable environmental parameters, J. Adhes. Sci. Technol. 29 (2014) 392–423, https://doi.org/10.1080/01694243.2014.958781.

[30] M.H. Nazir, Z.A. Khan, A. Saeed, K. Stokes, Modeling the effect of residual and diffusion-induced stresses on corrosion at the interface of coating and substrate, Corrosion 71 (6) (2015) 630–641, https://doi.org/10.5006/1556-2227-71.6.630.

[31] M.H. Nazir, Z.A. Khan, K. Stokes, Optimisation of interface roughness and coating thickness to maximise coating-substrate adhesion - A failure prediction and reliability assessment modelling, J. Adhes. Sci. Technol. 29 (2015) 1415–1445, https://doi.org/10.1080/01694243.2014.1000360.

[32] A. Saeed, Z.A. Khan, M.H. Nazir, Time dependent surface corrosion analysis and modelling of automotive steel under a simplistic model of variations in environmental parameters, Mater. Chem. Phys. 178 (2016) 65–73, https://doi.org/10.1016/j.matchemphys.2016.05.015.

[33] M. Nazir, Z.A. Khan, K. Stokes, A unified mathematical modelling and simulation for cathodic blistering mechanism incorporating diffusion and fracture mechanics concepts, J. Adhes. Sci. Technol. 29 (2015) 1200–1228, https://doi.org/10.1080/01694243.2015.1017497.

[34] M.H. Nazir, Z.A. Khan, K. Stokes, Analysing the coupled effects of compressive and diffusion induced stresses on the nucleation and propagation of circular coating blisters in the presence of micro-cracks, Eng. Fail. Anal. 70 (2016) 1–15, https://doi.org/10.1016/j.engfailanal.2016.07.016.

[35] M.H. Nazir, A. Saeed, Z. Khan, A comprehensive predictive corrosion model incorporating varying environmental gas pollutants applied to wider steel applications, Mater. Chem. Phys. 193 (2017) 19–34, https://doi.org/10.1016/j.matchemphys.2017.01.017.

[36] M. Nazir, Z. Khan, A review of theoretical analysis techniques for cracking and corrosive degradation of film-substrate systems, Eng. Fail. Anal. (2016).

[37] R. Bajwa, Z. Khan, H. Nazir, V. Chacko, A. Saeed, Wear and friction properties of electrodeposited ni-based coatings subject to nano-enhanced lubricant and composite coating, Acta Metall. Sin. (Engl. Lett.) 29 (2016) 902–910, https://doi.org/10.1007/s40195-016-0465-9.

[38] M.H. Nazir, Z. Khan, Maximising the interfacial toughness of thin coatings and substrate through optimisation of defined parameters, Int. J. Comput. Methods Exp. Meas. 3 (2015) 316–328, https://doi.org/10.2495/CMEM-V3-N4-316-328.

[39] R.S. Bajwa, Z. Khan, V. Bakolas, W. Braun, Effect of bath ionic strength on adhesion and tribological properties of pure nickel and Ni-based nanocomposite coatings, J. Adhes. Sci. Technol. 30 (2016) 653–665, https://doi.org/10.1080/01694243.2015.1112846.

[40] R.S. Bajwa, Z. Khan, V. Bakolas, W. Braun, Water-Lubricated Ni-Based Composite (Ni–Al2O3, Ni–SiC and Ni–ZrO2) Thin Film Coatings for Industrial Applications, Acta Metall. Sin. (Engl. Lett.) 29 (2015) 8–16, https://doi.org/10.1007/s40195-015-0218-7.

[41] M.H. Nazir, et al., Analyzing and modelling the corrosion behavior of Ni/Al2O3, Ni/SiC, Ni/ZrO2 and Ni/Graphene nanocomposite coatings, Materials 10 (2017) 1225, https://doi.org/10.3390/ma10101225.

[42] Z.A. Khan, M. Grover, M.H. Nazir, The implications of wet and dry turning on the surface quality of EN8 steel. Transactions on Engineering Technologies, Springer, 2015, pp. 413–423, https://doi.org/10.1007/978-94-017-7236-5_30.

[43] Z.A. Khan, V. Chacko, H. Nazir, A review of friction models in interacting joints for durability design, Friction 5 (2017) 1–22, https://doi.org/10.1007/s40544-016-0105-3.
[44] Z.A. Khan, H. Nazir, A. Saeed, Corrosion measurement device, Google Patents (2020). [No DOI available for patents.].
[45] J. Latif, Z.A. Khan, M.H. Nazir, K. Stokes, R. Smith, An optimal condition-based maintenance scheduling for metal structures based on a multidisciplinary research approach, Struct. Infrastruct. Eng. 15 (2019), https://doi.org/10.1080/15732479.2018.1554176.
[46] J. Latif, Z.A. Khan, M.H. Nazir, K. Stokes, J. Plummer, Condition monitoring and predictive modelling of coating delamination applied to remote stationary and mobile assets, Struct. Health Monit. 18 (2019) 1056–1073, https://doi.org/10.1177/1475921718806899.
[47] A. Savin, et al., Damage detection of carbon reinforced composites using nondestructive evaluation with ultrasound and electromagnetic methods, IOP Conf. Ser.: Mater. Sci. Eng. 133 (2016) 012013, https://doi.org/10.1088/1757-899X/133/1/012013.
[48] M.H. Nazir, Z.A. Khan, A. Saeed, V. Bakolas, W. Braun, R. Bajwa, Experimental analysis and modelling for reciprocating wear behaviour of nanocomposite coatings, Wear 416 (2018) 89–102, https://doi.org/10.1016/j.wear.2018.01.016.
[49] S.I. Novikova, Thermal expansion of solids, Mosc. Izd. Nauka 1 (1974).
[50] Y. Sakamoto, E. Kakihisa, Y. Kinari, Absorption of hydrogen by Pd-Al and Pd-In solid solution alloys, Z. F. üR. Phys. Chem. 179 (1993) 69–75, https://doi.org/10.1524/zpch.1993.179.Part_1_2.069.
[51] C. Stickels, P. Mould, The use of Young's modulus for predicting the plastic-strain ratio of low-carbon steel sheets, Metallurgical and, Mater. Trans. 1 (1970) 1303–1312, https://doi.org/10.1007/BF02900224.
[52] A.G. Evans, D. Mumm, J. Hutchinson, G. Meier, F. Pettit, Mechanisms controlling the durability of thermal barrier coatings, Prog. Mater. Sci. 46 (2001) 505–553, https://doi.org/10.1016/S0079-6425(00)00020-7.
[53] Y. Huang, H. Gao, W. Nix, J. Hutchinson, Mechanism-based strain gradient plasticity—II. Analysis, J. Mech. Phys. Solids 48 (2000) 99–128, https://doi.org/10.1016/S0022-5096(99)00079-0.
[54] V. Tvergaard, J.W. Hutchinson, The influence of plasticity on mixed mode interface toughness, J. Mech. Phys. Solids 41 (1993) 1119–1135, https://doi.org/10.1016/0022-5096(93)90072-3.
[55] F. Yang, J. Li, Diffusion-induced beam bending in hydrogen sensors, J. Appl. Phys. 93 (2003) 9304–9309, https://doi.org/10.1063/1.1572549.
[56] B.P. Van Milligen, P. Bons, B.A. Carreras, R. Sánchez, On the applicability of Fick's law to diffusion in inhomogeneous systems, Eur. J. Phys. 26 (2005) 913, https://doi.org/10.1088/0143-0807/26/6/003.
[57] L. Mejlbro, The complete solution of Fick's second law of diffusion with time-dependent diffusion coefficient and surface concentration, in: P. Sandberg (Ed.), Durability of Concrete in Saline Environment, Lund, 1996, pp. 127–158, https://doi.org/10.1007/978-3-540-28587-2_9.
[58] O.D. Kellogg, Foundations of Potential Theory, New York, (1929). [No DOI available].
[59] M.H. Nazir, Z.A. Khan, K. Stokes, Optimisation of interface roughness and coating thickness to maximise coating-substrate adhesion - a failure prediction and reliability assessment modelling, J. Adhes. Sci. Technol. (2015), https://doi.org/10.1080/01694243.2015.1026870.
[60] C.-H. Hsueh, Modeling of elastic deformation of multilayers due to residual stresses and external bending, J. Appl. Phys. 91 (2002) 9652–9656, https://doi.org/10.1063/1.1474870.
[61] F.-Z. Xuan, L.-Q. Cao, Z. Wang, S.-T. Tu, Mass transport in laser surface nitriding involving the effect of high temperature gradient: Simulation and experiment, Comput. Mater. Sci. 49 (2010) 104–111, https://doi.org/10.1016/j.commatsci.2010.01.003.
[62] X. Zhang, W. Shyy, A.M. Sastry, Numerical simulation of intercalation-induced stress in Li-ion battery electrode particles, J. Electrochem. Soc. 154 (2007) A910–A916, https://doi.org/10.1149/1.2737731.
[63] J. Hutchinson, M. Thouless, E. Liniger, Growth and configurational stability of circular, buckling-driven film delaminations, Acta Metall. Et. Mater. 40 (1992) 295–308, https://doi.org/10.1016/0956-7151(92)90039-B.
[64] T.Q. Lu, W.X. Zhang, T. Wang, The surface effect on the strain energy release rate of buckling delamination in thin film–substrate systems, Int. J. Eng. Sci. 49 (2011) 967–975, https://doi.org/10.1016/j.ijengsci.2011.01.003.
[65] L. Yao, R. Alderliesten, M. Zhao, R. Benedictus, Discussion on the use of the strain energy release rate for fatigue delamination characterization, Compos. Part A: Appl. Sci. Manuf. 66 (2014) 65–72, https://doi.org/10.1016/j.compositesa.2014.09.006.
[66] J.W. Hutchinson, M. Mear, J.R. Rice, Crack paralleling an interface between dissimilar materials, J. Appl. Mech. 54 (1987) 828–832, https://doi.org/10.1115/1.3172783.
[67] J.W. Hutchinson, Mixed mode fracture mechanics of interfaces, Met. Ceram. Interfaces (1990) 295–306, https://doi.org/10.1007/978-1-4757-5407-2_21.
[68] S. Schmauder, M. Meyer, Correlation between Dundurs' parameters and elastic constants, Z. F. üR. Metallkd. 83 (1992) 524–527, https://doi.org/10.3139/146.110030.
[69] T. Pardoen, J. Hutchinson, An extended model for void growth and coalescence, J. Mech. Phys. Solids 48 (2000) 2467–2512, https://doi.org/10.1016/S0022-5096(00)00042-1.
[70] Y. Cao, J.W. Hutchinson, From wrinkles to creases in elastomers: the instability and imperfection-sensitivity of wrinkling, Proc. R. Soc. Lond. A: Math., Phys. Eng. Sci. 468 (2012) 94–115, https://doi.org/10.1098/rspa.2011.0231.
[71] T. Kato, Perturbation Theory for Linear Operators, Springer Science & Business Media, 2012, https://doi.org/10.1007/978-3-642-21915-0.
[72] G. Xu, L. Yang, Y. Zhou, Q. Zhou, Failure mechanisms of thermal barrier coatings under thermo-mechanical-chemical loads. Thermal Barrier Coatings, Elsevier, 2023, pp. 361–432, https://doi.org/10.1016/B978-0-323-88286-7.00014-2.
[73] F. Jing, Y. Li, J. Zhang, Quantitative characterization of the interfacial damage in EB-PVD thermal barrier coating, Coatings 12 (2022) 984, https://doi.org/10.3390/coatings12070984.